J Mater Sci: Mater Electron

Determination of surface morphology and electrical properties of MoO_3 layer deposited on GaAs substrate with RF magnetron sputtering

Çağlar Çetinkaya[1,2], Erman Çokduygulular[3], Yunus Özen[2,4], İdris Candan[5], Barış Kınacı[1,2,*], and Süleyman Özçelik[2,6]

[1] Department of Physics, Faculty of Science, Istanbul University, 34134 Istanbul, Turkey
[2] Photonics Research Center, Gazi University, 06500 Ankara, Turkey
[3] Engineering Sciences, Faculty of Engineering, Istanbul University – Cerrahpasa, 34320 Istanbul, Turkey
[4] Department of Physics, Faculty of Science, Gazi University, 06500 Ankara, Turkey
[5] Department of Physics, Kocaeli University, 41001 İzmit, Kocaeli, Turkey
[6] Department of Photonics, Gazi University, 06500 Ankara, Turkey

Received: 12 November 2020
Accepted: 29 March 2021

© The Author(s), under exclusive licence to Springer Science+Business Media, LLC, part of Springer Nature 2021

ABSTRACT

We report the effects of the substrate temperature on the surface morphology of Molybdenum tri-oxide (MoO_3) thin films and the electrically detailed examination of Au/MoO_3/n–GaAs MOS heterojunction structure with the best homogeneity. MoO_3 thin film was deposited both on soda–lime silicate glass as a thin film and n-type and (100) oriented GaAs substrates using RF magnetron sputtering method at substrate temperatures of room temperature, 100 °C, 200 °C and 300 °C. Surface morphology of the MoO_3 thin films were investigated by utilizing atomic force microscopy (AFM) and scanning electron microscopy (SEM) measurements. AFM and SEM results have shown that MoO_3 thin film with substrate temperature of 200 °C has the lowest surface roughness and the homogeneity of the film structures significantly enhances with increasing substrate temperature up to 200 °C. An inclement in roughness of thin film structure was detected at higher temperature than 200 °C due to the deterioration of homogeneity. Therefore, we primarily focused on the MoO_3 thin films produced at the substrate temperature of 200 °C to examine the electrical properties of Au/MoO_3/n–GaAs MOS heterojunction device. In order to determine the electrical properties, temperature dependent $I-V$ measurements were performed in between 200 and 400 K by steps of 25 K. The fundamental electrical parameters such as saturation current (I_0), ideality factor (n), and barrier height (ϕ_0) were calculated by analyzing the forward bias $I-V$ curves at different temperatures. The series resistance (R_s) values of the device were also determined using the plot of structure resistance (R_i) vs applied bias voltage (V_i), Thermionic Emission Theory and Cheung and Cheung methods. The R_s

Address correspondence to E-mail: baris.kinaci@istanbul.edu.tr

https://doi.org/10.1007/s10854-021-05863-0
Published online: 09 April 2021

value of Au/MoO_3/n–GaAs MOS heterojunction device shows an abnormal behavior of up to 350 K, which is the critical temperature value and tends to increase with increasing temperature. Above the critical temperature value, it exhibits ideal behavior.

1 Introduction

Traditional transition metal-oxide (TMO) based thin films like molybdenum tri-oxide (MoO_3), vanadium pent-oxide (V_2O_5), or tungsten tri-oxide (WO_3) play a significant role in the optoelectronic and electronic devices for decades. They form an interfacial layer to modify charge transport properties, align favorable energy level, increase stability in especially organic photovoltaic technology and improve device performance of organic, inorganic, and hybrid structures [1–3]. The interest in TMO thin films is increasing day by day due to their ability to be integrated into structures designed for the new generation technology, high transparency values, being available as electrodes in various structures and being able to be used as a charge generation/recombination materials [4, 5]. In particular, the privilege of controlling the interface properties of TMO thin films has made them a promising material to the development of new generation optoelectronic devices [6]. Among the TMO materials, MoO_3 is the most widely used material because it has shown a variety of technological applications for electronic and optoelectronic technology such as organic [7] and perovskite solar cells [8], organic light emitting devices [4, 9, 10], gas and chemical sensors [11, 12], storage devices [13], lithium-ion and sodium-ion batteries [14, 15]. The reason for the widespread use of MoO_3 thin films is not only the superior electronic properties they show, but also that they can be produced with easy production and storage processes. For instance, the evaporation temperatures of V_2O_5 and WO_3 thin films are very high. On the other hand, MoO_3 thin films can be evaporated at relatively lower temperatures ($\sim$ 400 °C) and thus easily accumulated from a crucible in a high vacuum-free chamber. In this way, excessive release of oxygen and the uncontrolled heating of the substrate to be coated can be significantly prevented [4]. Moreover, numerous deposition techniques have been reported in the literature for the formation of MoO_3 like thermal evaporation [16–20], sputtering [21–25], pulsed laser deposition [26, 27], chemical vapor deposition [28, 29], atomic layer deposition [30], electrodeposition [31, 32], and spray pyrolysis [33] techniques. Among these deposition techniques, sputtering system is properly made use of due to its ability to obtain uniform, dense, and exact stoichiometric thin films [34–36].

Especially more recently, the studies on MoO_3 based devices with technologically important III/V-group semiconductors like Si and GaAs used as substrates continue increasingly. Si and GaAs wafers are the most widely used for modern semiconductor device technologies because they are still highly compatible with integrated circuits. The crystal structure of MoO_3 thin film fabricated using the RF magnetron sputtering method depends completely on the fabrication temperature [37]. Fan et al. reported that MoO_3 thin films fabricated at a substrate temperature of 200 °C or below this temperature are naturally amorphous while thin films showed the presence of monoclinic Mo_9O_{26} and orthorhombic MoO_3 at substrate temperatures of 300 °C and 400 °C, respectively [37, 38]. Furthermore, it has significantly enhanced the energy conversion efficiency of amorphous-Si based solar cells with electron extraction using MoO_3 electrodes [39–41]. In particular, MoO_3 as interfacial layer has become a unique material system for metal–oxide–semiconductor (MOS) heterojunction based Schottky device applications, where interface control is of great importance in metal–semiconductor contact due to its unique electrical, optical and structural properties. In order to design and promote the new generation electronic and optoelectronic devices, it is also very important to figure out the physics of hybrid structures formed by technologically crucial III/V-semiconductor substrate of GaAs and TMO materials. GaAs is perfectly convenient for efficient absorbance and emission of light because it is a direct-bandgap semiconductor [42, 43]. Furthermore, GaAs exhibits excellent electronic properties necessary for high-speed and radio-frequency devices due to the low effective mass of its carriers [44]. Therefore, the hybrid technology based on the integration of MoO_3 and GaAs serves up

prospects for advancing device technology because of these important technologically applicability. For instance, high efficiency GaAs based solar cells can be developed and tunable resistive electronic components can be produced due to the high ionization energy of MoO_3 and transparent [44]. In the literature, detailed studies have been made recently on interface properties of MoO_3/GaAs heterojunction hybrid structure by Ashraf et al. [44, 45]. They investigated the surface and interface structures of thin MoO_3/GaAs, effects of growth temperature and post-growth annealing on interface formation and the structure of MoO_3 as a thin film. These studies include only structural and morphological investigations, and there is no electrical and morphological comparative study on MoO_3/GaAs heterojunction MOS hybrid structure in the literature.

In this investigation, MoO_3 thin film as an interfacial layer was studied to figure out the effects of electronic properties and the surface morphology on the MoO_3/GaAs heterojunction structure. MoO_3 thin film layer was fabricated onto n type-GaAs substrate using RF magnetron sputtering method. We focus mainly on the examination and interpretation of the effect of different substrate temperatures on electrical properties and morphological changes in MoO_3/GaAs MOS heterojunction structure, which form the basis of many modern and innovative electronic and optoelectronic devices. In accordance with this purpose, we performed systematically atomic force microscope (AFM), scanning electron microscope (SEM) and current–voltage ($I - V$) measurements on MoO_3/GaAs heterojunction MOS hybrid structure by growth with different substrate temperature in between 200 and 400 K by step of 25 K.

2 Materials and methods

The MoO_3 thin films were deposited both on soda–lime silicate glass as a thin film and (100)-oriented n-type GaAs substrate using RF magnetron sputtering method. Before the deposition process, the surface of GaAs wafer and soda–lime silicate glass were subjected to a chemical cleaning procedure to remove contaminations. After the cleaning procedure, the GaAs substrate, soda–lime silicate glass, and MoO_3 target were loaded into the sputtering system. The distance between target and substrates was about 35 mm. When a base pressure of 10^{-6} mbar was reached, a 15 nm thin layer of MoO_3 film was deposited on well-cleaned substrates with the deposition rate of 0.2 Å/s. In order to figure out how to affect the substrate temperature to the electronic properties and the surface morphology on the MoO_3/GaAs heterojunction structure, four different samples were prepared by means of changing the substrate temperatures. The substrates' temperatures were maintained at room temperature (RT), 100 °C, 200 °C, and 300 °C, respectively.

The surface morphology of the films was analyzed utilizing high performance AFM (hp–AFM) (NanoMagnetics Instruments Ltd., Oxford, UK) with dynamic mode scanning at scan area of 3×3 μm^2 and JEOL JSM–7001F SEM at scan area of 1 μm^2. The root mean square (RMS) and grain size values of the films were obtained by analyzing AFM images.

In order to the electrical characterization of the structure at 200 °C substrate temperature, an ohmic back contact was initially formed by deposition of 200 nm thick AuGeNi at 350 °C. Afterwards, post-annealing process was carried out at 350 °C to obtain good ohmic contact behavior. Finally, the fabrication of the MoO_3/n–GaAs/AuGeNi heterojunction structure was completed with square–shaped rectifier contacts (2 mm diameter, 200 nm) deposition of high-purity Au (99.999%) coated on the front surface of the MoO_3 film structure. I–V measurements with the forward and reverse bias were carried out in the temperature range 200–400 K using a Keithley 2400 source meter. The temperature was adjusted using Janisvpf-475 cryostat and a Lake Shore model 321 auto-tuning temperature controllers.

3 Results and discussion

In order to investigate the effect of substrate temperature on the surface morphology and to determine the best surface homogeneity of the MoO_3 thin films, AFM and SEM measurements were carried out for the MoO_3 thin films deposited on soda–lime silicate glass as a thin film at substrate temperature with RT, 100 °C, 200 °C and 300 °C. Figure 1a–d illustrate the three–dimensional (3D) AFM images of the MoO_3 thin film with different substrate temperatures (RT, 100 °C, 200 °C and 300 °C).

Surface morphology and roughness of MoO_3 thin films were evaluated based on AFM measurements with a scan area of 3×3 μm^2. The surface roughness

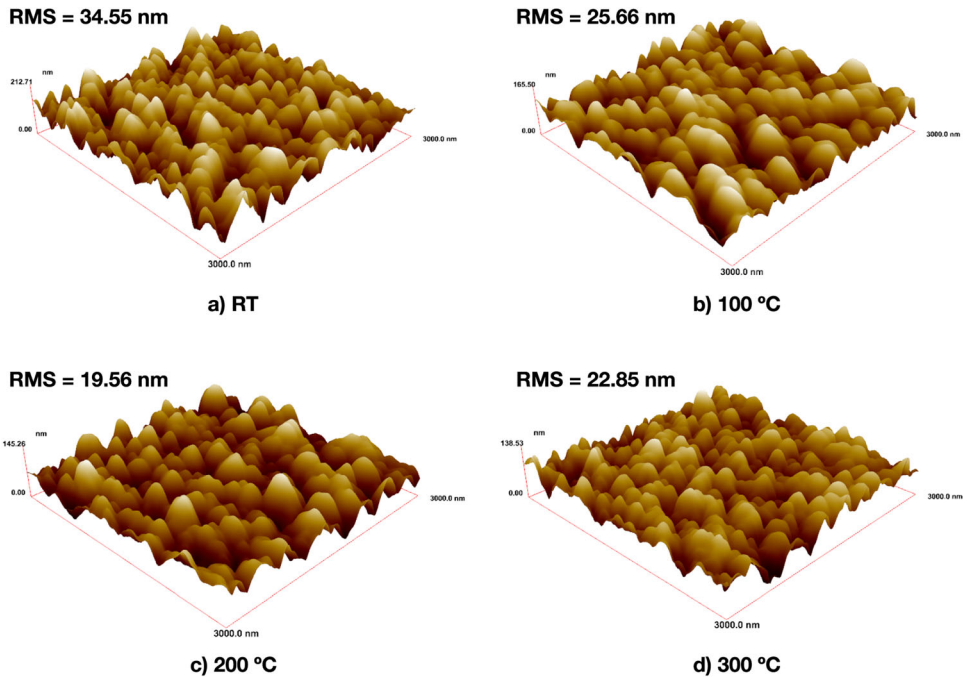


Fig. 1 3×3 μm^2 AFM image of MoO_3 thin films at substrate temperatures of **a** RT, **b** 100 °C, **c** 200 °C and **d** 300 °C

(in Root Mean Square, RMS) of the MoO_3 thin films grown at different substrate temperatures were found as 34.55 nm, 26.66 nm, 19.56 nm and 22.85 nm for RT, 100 °C, 200 °C and 300 °C, respectively. As clearly seen from Fig. 1, the MoO_3 thin film deposited at substrate temperature of 200 °C has the lowest surface roughness. Moreover, the homogeneity of the MoO_3 thin films enhanced with increasing substrate temperature up to 200 °C. After this temperature value, an inclement in roughness was observed as the thin film homogeneity deteriorated.

SEM images of the MoO_3 thin films coated at different substrate temperatures are presented in Fig. 2a–d. The surface of MoO_3 thin film grown at RT substrate temperature is not uniform and prominent as can be seen in Fig. 2a. However, it was observed that the surface becomes fairly homogeneity as substrate temperature increase up to 200 °C, which is quite well consistent with the result of AFM images. This situation can be attributed to optimum MoO_3 thin film formation on the substrate at temperature of 200 °C. When the substrate temperature is raised to 200 °C, the surface topography of the MoO_3 thin film is flatter and uniform without any small gains. After this temperature, the surface of MoO_3 thin film starts to lose its homogeneity as seen from Fig. 2d.

Analysis of AFM and SEM measurements showed that MoO_3 thin film coated at the substrate temperature of 200 °C has the best surface homogeneity. Therefore, it can be a strong candidate to use as an interface layer in new generation MIS/MOS electronic and optoelectronic devices. Hence, we primarily focused on the MoO_3 thin film deposited on n–type GaAs substrate at the substrate temperature of 200 °C to examine the electrical properties that are crucial for device applications. In order to understand the electrical properties of Au/MoO_3/n–GaAs MOS devices for MoO_3 thin film sample produced at the temperature value of 200 °C, temperature dependent $I-V$ measurements were performed in the temperature range 200–400 K. The fundamental electrical parameters like saturation current (I_0), ideality factor (n) and barrier height (ϕ_0) were calculated using the following well–known equation [46–48];

$$I = I_0\left[e^{\left(\frac{qV}{nk_BT}\right)} - 1\right] \tag{1}$$

Here I_0 is the reverse saturation current and derived from the straight-line fitting at a zero bias, V is the bias voltage, n is the diode ideality factor and k_B is the Boltzman constant and T is the operating temperature in Kelvin. The reverse saturation current of I_0 is expressed by the following relation:

$$I_0 = AA^*T^2e^{-\left(\frac{q\phi_{b0}}{k_BT}\right)} \tag{2}$$

where A is the diode area, A^* is the Richardson

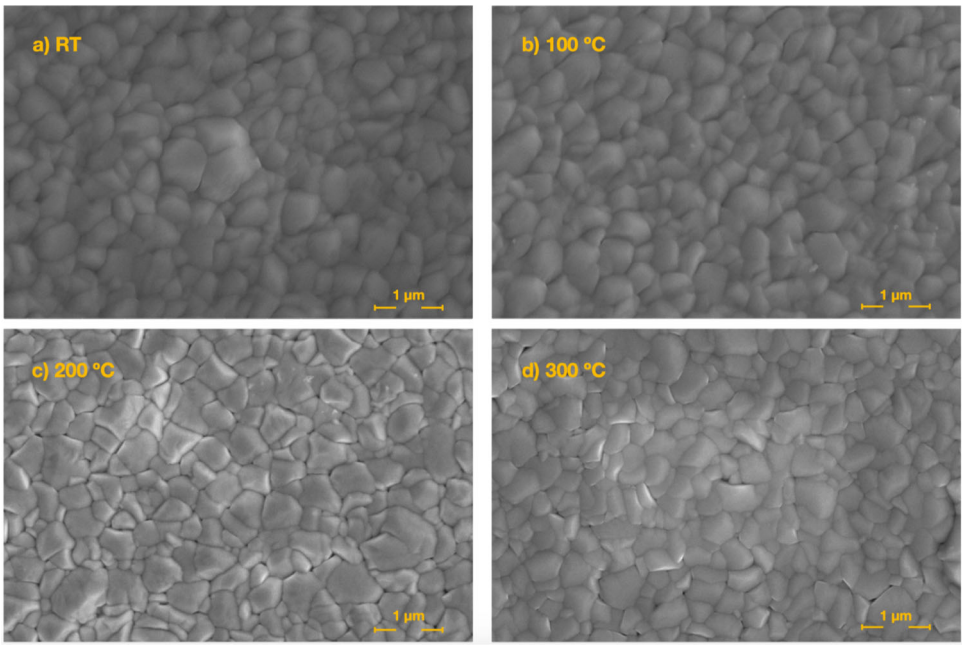


Fig. 2 SEM image of MoO_3 thin films in 1 μm at substrate temperatures of **a** RT, **b** 100 °C, **c** 200 °C and **d** 300 °C

constant which is 8.16 Acm^2K^{-2} for n-type GaAs [47, 49, 50], q is the electron charge. The ideality factor is described the deviation of experimental $I-V$ data from the Thermionic Emission (TE) Theory. The definition of ideality factor is given by the equation:

$$n = \frac{q}{k_B T}\frac{dV}{d\ln(I)} \tag{3}$$

n is one of the most important parameters for diode uniformity and is equal to 1 for an ideal diode, but in practice, n is greater than 1 for a real situation. Generally, the value of n is expected to be greater than 1 because of the barrier inhomogeneity at metal–semiconductor interface and the presence of interface thin layer of MoO_3 film. On the other hand, ϕ_0 can be obtained from Eq. (2) as:

$$\phi_{b0} = \frac{k_B T}{q}\ln\left(\frac{AA^* T^2}{I_0}\right) \tag{4}$$

The forward and reverse bias $I-V$ curves of Au/n–GaAs structure with MoO_3 interfacial layer in the temperature range of 200–400 K are given in Fig. 3. As seen from Fig. 3, $I-V$ curves are linear at low forward bias voltages (in the range of 0–1 V) and the curves deviate from linearity at high forward bias region (greater than 1 V). This deviation is due to the existence of the series resistance (R_s), barrier inhomogeneity, and interface states (N_{ss}).

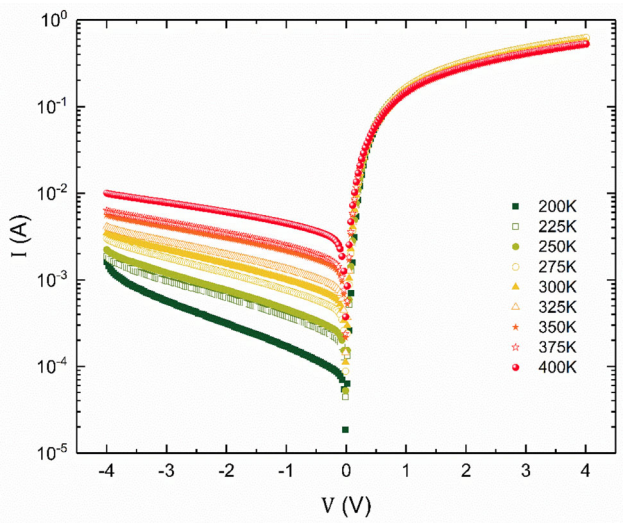


Fig. 3 Forward and reversed bias $I-V$ characteristics of Au/MoO_3/n–GaAs MOS heterojunction structure fabricated at substrate temperature of 200 °C in the temperature range of 200–400 K

The values of n and ϕ_0 for Au/n–GaAs structure with MoO_3 interfacial layer vary from 6.25 and 0.25 eV (at 200 K) to 3.52 and 0.57 eV (at 400 K), respectively. Figure 4 shows the variation in values of n and ϕ_0 for the temperature range of 200–400 K. As given in Fig. 4, the calculated values of n decrease with increasing temperature while the calculated values of ϕ_0 increase with increasing temperature values. It is also seen in the figure that the barrier

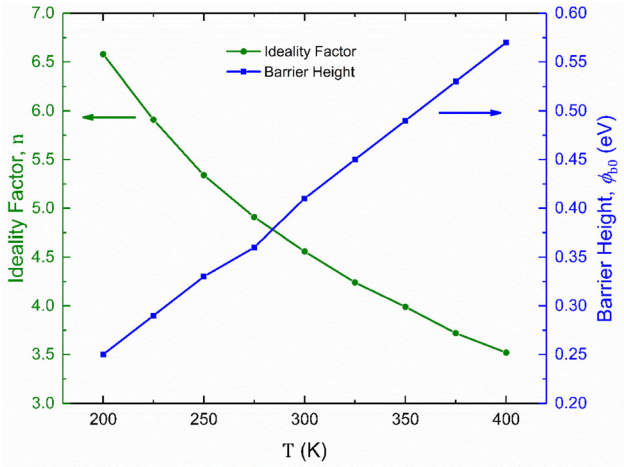


Fig. 4 Ideality factor and barrier height of Au/MoO_3/n–GaAs MOS heterojunction structure in the temperature range of 200–400 K

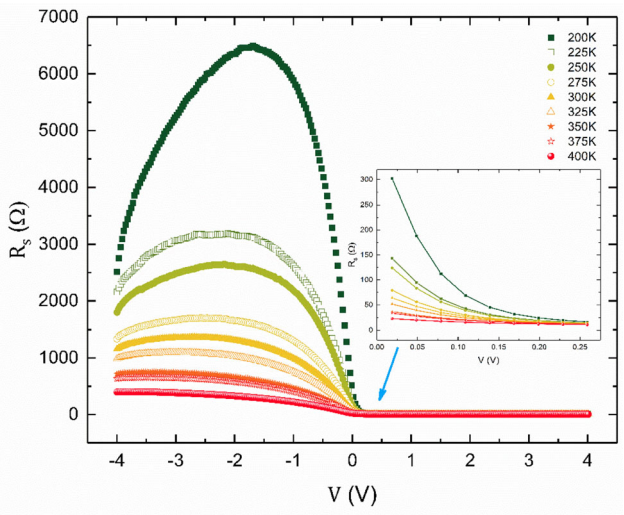


Fig. 5 Serial resistance–voltage characteristics of Au/MoO_3/n–GaAs MOS heterojunction structure in the temperature range of 200–400 K. Inset shows the changing in R_s values as a function of the forward bias voltage in between 0 and 0.25 V

height value increases linearly with increasing temperature. This result clearly highlights the inhomogeneity of barrier height. According to thermionic emission (TE) theory, this linear rise in the barrier height with increasing temperature shows that there are inhomogeneities at the metal/semiconductor (MS) interface [51–53]. Correspondingly, the ϕ_0 for current transport decreased and the n increased at low temperatures due to the deviation of a Schottky barrier from pure thermionic emission. On the other hand, the increase in ϕ_0 with increasing temperature is due to temperature-activated current transport across the MS interface. Therefore, this behavior of ϕ_0 and n with temperature to Schottky barrier homogeneities has been attributed to assuming the Gaussian distribution of barrier heights at the MS interface and the Richardson plot shows good linearity over the temperature range [51–53]. Additionally, the existence of MoO_3 thin film as interfacial layer can affect the current conduction and barrier homogeneity in between metal and semiconductor. Mahoto et al. have reported that bandgap value of TMO layer increased when temperature decreased and the charge carriers cannot have enough energy to overcome the barrier height at low temperatures [6]. Therefore, in this study, we focused on the temperature range of 200–400 K.

The series resistance (R_s), one of the important parameters of MIS or MOS structures, was computed from the structure resistance (R_i) and applied bias voltage (V_i). The structure resistance derived from $I-V$ graph using $R_i = \frac{dV_i}{dI_i}$ relation. Figure 5 shows the calculated series resistance of Au/MoO_3/n–GaAs MOS heterojunction in the temperature range of 200–400 K. Figure inset presents the changing in R_s values as a function of the forward bias voltage in between 0 and 0.25 V. As observed from Fig. 5, the structure's serial resistance values at sufficiently high forward bias voltage approach to a constant value. The temperature also affected the R_s values and they were calculated to be 6.88 Ω at temperature of 200 K and 7.65 Ω at temperature of 400 K. The temperature dependent values of the calculated R_s and other

Table 1 Temperature dependent electrical parameters of the Au/MoO_3/n–GaAs MOS heterojunction structure fabricated at substrate temperature of 200 °C in the temperature range of 200–400 K

T (K)	I–V characteristics			$dV/d\ln(I)$	$H(I)$
	n	$\phi_{b0}(eV)$	$R_s(\Omega)$	$R_s(\Omega)$	$R_s(\Omega)$
200	6.58	0.25	6.88	6.97	6.85
225	5.91	0.29	6.57	7.35	6.63
250	5.43	0.33	6.54	7.08	6.61
275	4.91	0.36	6.43	7.54	6.56
300	4.56	0.41	7.11	7.97	7.27
325	4.24	0.45	7.45	8.52	7.63
350	3.99	0.49	7.73	8.67	7.95
375	3.72	0.53	7.69	8.48	7.89
400	3.52	0.57	7.56	8.40	7.84

electrical parameters of the Au/MoO_3/n–GaAs MOS heterojunction device are given in Table 1. As clearly seen from Fig. 5 and Table 1, Au /n–GaAs structure with MoO_3 interfacial layer has very low R_s values. However, it shows an abnormal behavior of up to 350 K, which is the critical temperature, and tends to increase with increasing temperature. After this temperature value, it exhibits ideal behavior.

The series resistance values can be determined from the temperature dependent forward bias $I-V$ characteristics known as the Cheung and Cheung method [6, 46, 48–50, 54]. According to this method, current–voltage characteristics related to Thermionic Emission Theory can be expressed as follows:

$$\frac{dV}{d\ln(I)} = n\frac{k_BT}{q} + R_sI \tag{5}$$

Figure 6 shows $\frac{dV}{d\ln(I)}$ versus I curves that exhibit a linear behavior at different temperatures. The slope of the linear line gives the series resistance. The values of R_s obtained from this Figure to be 6.97 Ω at temperature of 200 K and 8.40 Ω at temperature of 400 K.

In order to obtain the series resistance from third way, the ideality factor values determined from the temperature dependent $I-V$ curves were also used in another equation of Cheung and Cheung. As a third way, another equation of Cheung and Cheung defined by the following relation:

$$H(I) = V - n\frac{k_BT}{q}\ln\left(\frac{I}{AA^*T^2}\right) = n\phi_{b0} + R_sI \tag{6}$$

The plots of $H(I)$ versus I in the temperatures range from 200 to 400 K are presented in Fig. 7. The values of R_s were calculated as 6.56 Ω at 200 K and 7.84Ω at 400 K from Fig. 7. The R_s values evaluated from the plots of $\frac{dV}{d\ln(I)}$ versus I are almost identical to those from the plot of $H(I)$ versus I graphs. These results confirm the consistency and validity of both models. The comparison of all calculated R_s values are given in Fig. 8. In addition, the values of series resistance obtained from temperature dependent $I-V$ curves are quite compatible with the values obtained from the Cheung functions as seen from Fig. 8. The temperature point of 350 K stands out as a critical temperature value. While R_s values obtained from all three curves up to 350 K almost tend to increase with increasing temperature value, they show a decreasing trend after this critical temperature value.

The presence of defects in the metal oxide layer is directly proportional to the temperature. They increase as the temperature increases and decrease as the temperature decreases. Similarly, the current passing through the defect level is directly proportional to the increasing in temperature during the transmission. Therefore, the defect states in the MoO_3 thin film layer affect the current flow mechanisms in the structure. However, in this study, it was observed

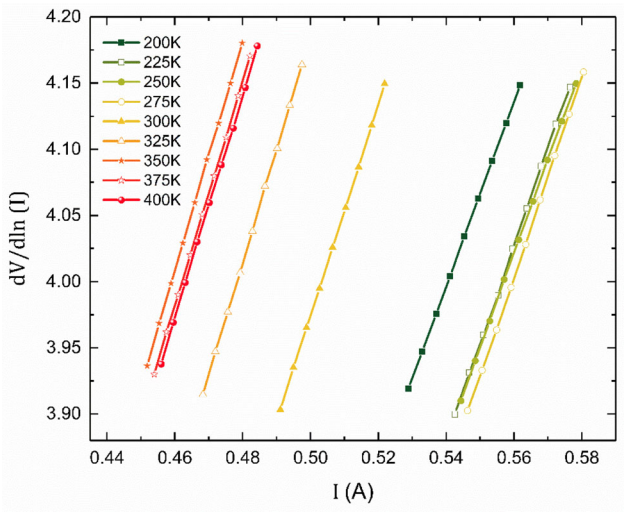


Fig. 6 The variation of $dV/d(\ln I) - I$ characteristics of Au/MoO_3/n–GaAs MOS heterojunction structure fabricated at the substrate temperature of 200 °C for different temperature values in between 200 and 400 K

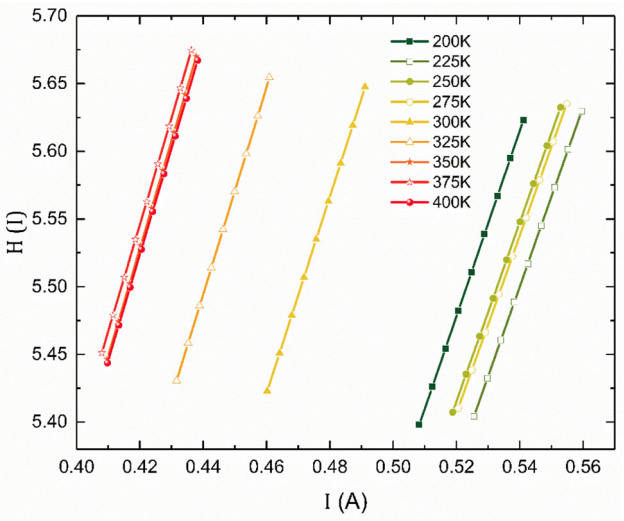


Fig. 7 The variation of $H(I) - I$ characteristics of Au/MoO_3/n–GaAs MOS heterojunction structure fabricated at the substrate temperature of 200 °C for different temperature values in between 200 and 400 K

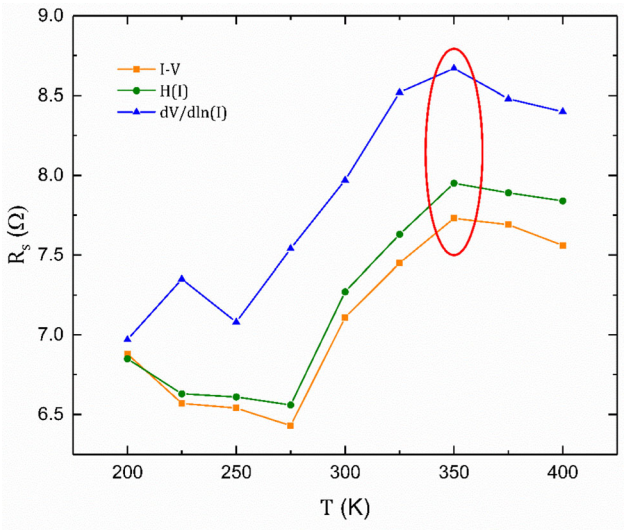


Fig. 8 The comparison of all calculated R_s values of MoO_3/n–GaAs MOS heterojunction structure fabricated at the substrate temperature of 200 °C in the temperature range of 200–400 K

for the MoO_3 thin film layer that the increasing in temperature up to the critical temperature value tended to increase in series resistance because the defect states up to the critical temperature value did not exhibit a dominant behavior in current transmission mechanisms. After the critical temperature value, the defect states started to dominate the current flow mechanisms. The experimental results indicated that R_s values of the Au/MoO_3/n–GaAs MOS heterojunction device exhibit unusual behavior. They increase with increasing temperature up to critical temperature value, and then, the R_s values exhibit expected behavior due to the effect of the defect states.

4 Conclusion

In this study, the effect of MoO_3 thin film as an interfacial layer on the Au/MoO_3/n–GaAs MOS heterojunction structure was investigated in terms of substrate temperature. The MoO_3 thin films were grown both on soda–lime silicate glass as a thin film and n–type GaAs substrates using RF sputter system at different substrate temperatures. The surface morphology of the MoO_3 thin films with different substrate temperatures was determined by conducting AFM and SEM measurements. Experimental results show that the thin film with substrate temperature of 200 °C has the best surface homogeneity and an inclement in roughness was detected as thin film homogeneity deteriorated at higher temperatures than 200 °C. MoO_3 thin films show these properties at a much lower substrate temperature compared to other TMO materials. This property of MoO_3 thin films makes them a strong candidate as an interface layer in new generation MIS/MOS electronic and optoelectronic devices. Hence, we focused on the examination of crucial electrical properties in new generation device applications using MoO_3 produced on n–type GaAs substrates at low substrate temperature. In order to obtain electrical properties of devices, temperature–dependent current–voltage ($I-V$) characterization in the temperature range of 200 K to 400 K by step 25 K was examined. The fundamental electrical parameters like I_0, n and ϕ_0 were calculated by analyzing the forward bias $I-V$ curve. The values of n and ϕ_0 for Au/MoO_3/n–GaAs MOS heterojunction structure vary from 6.25 and 0.25 eV at temperature of 200 K to 3.52 and 0.57 eV at temperature of 400 K, respectively. We found that n values decrease with increasing temperature, while ϕ_0 values increase with increasing temperature values as expected. In addition, we calculated R_s values of Au/n–GaAs structure with MoO_3 interfacial layer, which are very important for device applicability, using from both $I-V$ measurements and Cheung methods. The Au/MoO_3/n–GaAs structure fabricated at substrate temperature of 200 °C exhibits an unexpected behavior for R_s values up to 350 K, which is the critical temperature, due to whether the current transmission mechanisms are active or inactive. After this value, it decreases with increasing temperature, which is the ideal behavior. These results clearly highlight the potential of practical application of the Au/n–GaAs structure with MoO_3 interfacial layer to be used for new generation electronic and optoelectronic device applications.

Acknowledgements

This work was supported by Gazi University Photonics Research Center and the Directorate of Presidential Strategy and Budget of Turkey (Project No: 2019K12-92587).

References

1. C. Girotto, E. Voroshazi, D. Cheyns, P. Heremans, B.P. Rand, ACS Appl. Mater. Interfaces **3**, 3244 (2011)
2. A.L.F. Cauduro, R. Dos Reis, G. Chen, A.K. Schmid, C. Méthivier, H.G. Rubahn, L. Bossard-Giannesini, H. Cruguel, N. Witkowski, M. Madsen, ACS Appl. Mater. Interfaces **9**, 7717 (2017)
3. H. Simchi, B.E. McCandless, T. Meng, W.N. Shafarman, J. Alloys Compd. **617**, 609 (2014)
4. J. Meyer, S. Hamwi, M. Kröger, W. Kowalsky, T. Riedl, A. Kahn, Adv. Mater. **24**, 5408 (2012)
5. G. Sanal Kumar, N. Illyaskutty, S. Suresh, R.S. Sreedharan, V.U. Nayar, V.P.M. Pillai, J. Alloys Compd. **698**, 215 (2017)
6. S. Mahato, D. Biswas, L.G. Gerling, C. Voz, J. Puigdollers, AIP Adv. **7**, 085313 (2017)
7. N.K. Elumalai, A. Saha, C. Vijila, R. Jose, Z. Jie, S. Ramakrishna, Phys. Chem. Chem. Phys. **15**, 6831 (2013)
8. E.M. Sanehira, B.J. Tremolet de Villers, P. Schulz, M.O. Reese, S. Ferrere, K. Zhu, L.Y. Lin, J.J. Berry, J.M. Luther, ACS Energy Lett. **1**, 38 (2016)
9. C. Wang, I. Irfan, X. Liu, Y. Gao, J. Vac. Sci. Technol. B **32**, 053402 (2014)
10. M.C. Gwinner, R. Di Pietro, Y. Vaynzof, K.J. Greenberg, P.K.H. Ho, R.H. Friend, H. Sirringhaus, Adv. Funct. Mater. **21**, 1432 (2011)
11. M.B. Rahmani, S.H. Keshmiri, J. Yu, A.Z. Sadek, L. Al-Mashat, A. Moafi, K. Latham, Y.X. Li, W. Wlodarski, K. Kalantar-zadeh, Sens. Actuators B Chem. **145**, 13 (2010)
12. E. Comini, L. Yubao, Y. Brando, G. Sberveglieri, Chem. Phys. Lett. **407**, 368 (2005)
13. A.A. Bessonov, M.N. Kirikova, D.I. Petukhov, M. Allen, T. Ryhänen, M.J.A. Bailey, Nat. Mater. **14**, 199 (2015)
14. W. Chen, H. Zhang, Y. Wang, Z. Ma, Z. Li, Electrochim. Acta **144**, 369 (2014)
15. K. Zhu, X. Wang, J. Liu, S. Li, H. Wang, L. Yang, S. Liu, T. Xie, A.C.S. Sustain, Chem. Eng. **5**, 8025 (2017)
16. K. Koike, R. Wada, S. Yagi, Y. Harada, S. Sasa, and M. Yano, Jpn. J. Appl. Phys. **53**, 05FJ02 (2014).
17. S. Balendhran, J. Deng, J.Z. Ou, S. Walia, J. Scott, J. Tang, K.L. Wang, M.R. Field, S. Russo, S. Zhuiykov, M.S. Strano, N. Medhekar, S. Sriram, M. Bhaskaran, K. Kalantar-Zadeh, Adv. Mater. **25**, 109 (2013)
18. K. Kalantar-Zadeh, J. Tang, M. Wang, K.L. Wang, A. Shailos, K. Galatsis, R. Kojima, V. Strong, A. Lech, W. Wlodarski, R.B. Kaner, Nanoscale **2**, 429 (2010)
19. M. Itoh, K. Hayakawa, S. Oishi, J. Phys. Condens. Matter **13**, 6853 (2001)
20. C. Julien, A. Khelfa, O.M. Hussain, J. Cryst. Growth **156**, 235 (1995)
21. W.C. Chang, X. Qi, J.C. Kuo, S.C. Lee, S.K. Ng, D. Chen, CrystEngComm **13**, 5125 (2011)
22. C.V. Ramana, V.V. Atuchin, V.G. Kesler, V.A. Kochubey, L.D. Pokrovsky, V. Shutthanandan, U. Becker, R.C. Ewing, Appl. Surf. Sci. **253**, 5368 (2007)
23. H. Ohtsuka, Y. Sakurai, Jpn. J. Appl. Phys. **40**, 4680 (2001)
24. J.Y. Zou, G.L. Schrader, Thin Solid Films **324**, 52 (1998)
25. J. Okumu, F. Koerfer, C. Salinga, M. Wuttig, J. Appl. Phys. **95**, 7632 (2004)
26. M.A. Camacho-López, L. Escobar-Alarcón, E. Haro-Poniatowski, Appl. Phys. A Mater. Sci. Process. **78**, 59 (2004)
27. J. Torres, J.E. Alfonso, L.D. López-Carreño, Phys. Status Solidi C Conf. **2**, 3726 (2005)
28. A. Abdellaoui, G. Lévêque, A. Donnadieu, A. Bath, B. Bouchikhi, Thin Solid Films **304**, 39 (1997)
29. K. Hosono, I. Matsubara, N. Murayama, S. Woosuck, N. Izu, Chem. Mater. **17**, 349 (2005)
30. X. Liu, S. Yi, C. Wang, C. Wang, Y. Gao, J. Appl. Phys. **115**, 163508 (2014)
31. D. Di Yao, J.Z. Ou, K. Latham, S. Zhuiykov, A.P. O'Mullane, K. Kalantar-Zadeh, Cryst. Growth Des. **12**, 1865 (2012)
32. T.M. McEvoy, K.J. Stevenson, J.T. Hupp, X. Dang, Langmuir **19**, 4316 (2003)
33. P.R. Patil, P.S. Patil, Thin Solid Films **382**, 13 (2001)
34. E. Çokduygulular, Ç. Çetinkaya, Y. Yalçın, B. Kınacı, J. Mater. Sci. Mater. Electron. **31**, 13646 (2020)
35. F. Güzelçimen, B. Tanören, Ç. Çetinkaya, M.D. Kaya, H.İ Efkere, Y. Özen, D. Bingöl, M. Sirkeci, B. Kınacı, M.B. Ünlü, S. Özçelik, Vacuum **182**, 109766 (2020)
36. B. Kınacı, Ç. Çetinkaya, E. Çokduygulular, H.İ Efkere, N.A. Sönmez, S. Özçelik, J. Mater. Sci. Mater. Electron. **31**, 8718 (2020)
37. X. Fan, G. Fang, P. Qin, N. Sun, N. Liu, Q. Zheng, F. Cheng, L. Yuan, X. Zhao, J. Phys. D. Appl. Phys. **44**, 045101 (2011)
38. K. V. Alex, A. R. Jayakrishnan, S. AjeeshKumar, A. S. Ibrahim, K. Kamakshi, J. P. B. Silva, K. C. Sekhar, and M. J. M. Gomes, Mater. Res. Express **6**, 066421 (2019).
39. J. Geissbühler, J. Werner, S. Martin De Nicolas, L. Barraud, A. Hessler-Wyser, M. Despeisse, S. Nicolay, A. Tomasi, B. Niesen, S. De Wolf, C. Ballif, Appl. Phys. Lett. **107**, 081601 (2015)
40. C. Battaglia, X. Yin, M. Zheng, I.D. Sharp, T. Chen, S. McDonnell, A. Azcatl, C. Carraro, B. Ma, R. Maboudian, R.M. Wallace, A. Javey, Nano Lett. **14**, 967 (2014)
41. J. Bullock, A. Cuevas, T. Allen, C. Battaglia, Appl. Phys. Lett. **105**, 232109 (2014)
42. L.R. Weisberg, J. Appl. Phys. **39**, 6096 (1968)
43. K. Tomioka, J. Motohisa, S. Hara, K. Hiruma, T. Fukui, Nano Lett. **10**, 1639 (2010)

44. A. Sarkar, T. Ashraf, W. Grafeneder, R. Koch, J. Phys. Condens. Matter **30**, 155001 (2018)
45. T. Ashraf, A. Sarkar, W. Grafeneder, R. Koch, J. Appl. Phys. **124**, 215301 (2018)
46. B. Kınacı, S. ŞebnemÇetin, A. Bengi, S. Özçelik, Mater. Sci. Semicond. Process. **15**, 531 (2012)
47. O. Çiçek, H.U. Tecimer, S.O. Tan, H. Tecimer, S. Altindal, I. Uslu, Compos. Part B Eng. **98**, 260 (2016)
48. H.U. Tecimer, M.A. Alper, H. Tecimer, S.O. Tan, S. Altındal, Polym. Bull. **75**, 4257 (2018)
49. O. Çiçek, H.U. Tecimer, S.O. Tan, H. Tecimer, İ Orak, Ş Altındal, Compos. Part B Eng. **113**, 14 (2017)
50. S.O. Tan, H.U. Tecimer, O. Çiçek, H. Tecimer, İ Orak, Ş Altındal, J. Mater. Sci. Mater. Electron. **27**, 8340 (2016)
51. Y.P. Song, R.L. Van Meirhaeghe, W.H. Laflère, F. Cardon, Solid State Electron. **29**, 633 (1986)
52. R.T. Tung, Phys. Rev. B **45**, 13509 (1992)
53. A. BuyukbasUlusan, A. Tataroglu, Indian J. Phys. **92**, 1397 (2018)
54. S.K. Cheung, N.W. Cheung, Appl. Phys. Lett. **49**, 85 (1986)

Publisher's Note Springer Nature remains neutral with regard to jurisdictional claims in published maps and institutional affiliations.